

1 **Blue Flashes as Counterparts to Narrow Bipolar**
2 **Events: the Optical Signal of Shallow In-Cloud**
3 **Discharges**

4 **Dongshuai Li¹, Alejandro Luque¹, F. J. Gordillo-Vázquez¹, Feifan Liu²,**
5 **Gaopeng Lu², Torsten Neubert³, Olivier Chanrion³, Baoyou Zhu², Nikolai**
6 **Østgaard⁴, Víctor Reglero⁵**

7 ¹Instituto de Astrofísica de Andalucía (IAA), CSIC, Granada, Spain.

8 ²CAS Key Laboratory of Geospace Environment, School of Earth and Space Sciences, University of
9 Science and Technology of China, Hefei, China

10 ³National Space Institute, Technical University of Denmark (DTU Space), Kongens Lyngby, Denmark.

11 ⁴Birkeland Centre for Space Science, Department of Physics and Technology, University of Bergen,
12 Bergen, Norway

13 ⁵Image Processing Laboratory, University of Valencia, Valencia, Spain

14 **Key Points:**

- 15 • Negative-polarity NBEs are typically associated with extended optical sources at
16 the edge of a thundercloud.
17 • Thermal emissions in the oxygen 777 nm band are absent or very weak, indicat-
18 ing non-thermal processes.
19 • The optical energy in the 337 nm band is about 10^4 J, which requires around 10^9
20 streamers.

Corresponding author: Dongshuai Li, Alejandro Luque, dsl@iaa.es, aluque@iaa.es.
Instituto de Astrofísica de Andalucía (IAA), CSIC, Granada, Spain.

Abstract

Narrow Bipolar Events (NBEs) are powerful radio emissions from thunderstorms which have been recently associated with blue optical flashes on cloud tops and attributed to extensive streamer electrical discharges named fast breakdown. Combining data obtained from a thunderstorm over South China by the space-based Atmosphere Space Interactions Monitor (ASIM), the Vaisala GLD360 global lightning network and very low frequency (VLF)/low frequency (LF) radio detectors, here we report and analyze for the first time the optical emissions of Blue Luminous Events (BLUES) associated with negative NBEs and located at the top edge of a thundercloud. These emissions are weakly affected by scattering from cloud droplets, allowing us to estimate the source extension and optical energy involved in the process. The optical energy in the 337-nm band emitted by fast breakdown is about 10^4 J, which involves around 10^9 streamer initiation events.

Plain Language Summary

Installed on the International Space Station (ISS), the Atmosphere-Space Interactions Monitor (ASIM) is designed to observe Earth thunderstorms from space. Often it detects bursts of blue light emerging from active thunderclouds. These detections have been previously linked to radio signals named Narrow Bipolar Events (NBEs) that are routinely detected during a thunderstorm. Here we analyze the blue flashes from a storm that profusely produced negative-polarity NBEs. The optical signal can be understood as being produced by extended events close to the cloud top and we show that it is consistent with the barely understood electrical discharge process called fast breakdown that involves a huge number of thin, bright filaments called streamers.

1 Introduction

Blue Luminous Events (hereafter, BLUES), such as blue jets and blue starters, are transient electrical phenomena that occur in active thunderstorms and are characterized by optical signals strongly dominated by the blue range of the spectrum and lasting from about one millisecond to hundreds of milliseconds. They were first reported by Wescott et al. (1995, 1996) in the framework of the Sprites 1994 aircraft campaign. After these initial reports, BLUES have been observed and investigated mainly from space-based platforms: for example, from black-and-white camera of the Space Shuttle (Boeck et al., 1998), from the limb-pointing Imager of Sprites/Upper Atmospheric Lightning (ISUAL) onboard FORMOSAT-2 (Kuo et al., 2005; Chou et al., 2011, 2018), from off-the-shelf cameras on the International Space Station (ISS) (Chanrion et al., 2017) and, most recently, from the Modular Multispectral Imaging Array (MMIA) of the Atmosphere-Space Interactions Monitor (ASIM) onboard the ISS since April 2, 2018 (Soler et al., 2020; Neubert et al., 2021). BLUES can also be observed from the ground, as reported by Edens (2011), but this is complicated due to Rayleigh scattering and extinction by intervening clouds.

As we define them here, BLUES comprise several phenomena. Blue jets normally emerge out of the cloud top and reach altitudes about 40 km - 50 km at speeds of the order of 100 km/s (Wescott et al., 2001). Blue starters terminate at lower altitudes, typically around 18 km but sometimes up to 25 km and advance with velocities 10 km/s to 100 km/s (Wescott et al., 1996); they are often described as initial phases of blue jets (Pasko, 2008) and hence their name. Other types of BLUES have also been reported, including small blue surface discharges (sometimes called *blue glimpses*) that appear to “dance” on the upper layer of the cloud at a rate of about 120 per minute (Chanrion et al., 2017) and the *gnomes* that emerge directly from the cloud top within ~ 1 km, similar to blue starters, but with brighter and more uniform optical emission and much more compact shape (Lyons et al., 2003). *Giant jets*, which travel from cloud tops to the lower ionosphere, may also be classified as BLUES although they involve measurable emissions in the 777.4-nm band (van der Velde et al., 2019).

Each of these types of phenomena exhibits a different morphology but they likely share common physical processes. The blue color indicates the presence of electron-impact excitation of molecular nitrogen (Pasko, 2008; Surkov & Hayakawa, 2020; F. Gordillo-Vázquez & Pérez-Invernón, 2021) and the weak or absent atomic oxygen line at 777.4 nm, indicates that air does not reach high temperatures, typically associated with lightning leaders at ground level. This points to streamer coronas being the key component of BLUES, a conclusion supported by the close association between BLUES and Narrow Bipolar Events (NBEs) (F. Liu et al., 2018; Soler et al., 2020), which are radio emissions also attributed to corona discharges in thunderclouds (Rison et al., 2016; Tilles et al., 2019; N. Liu et al., 2019). It is thus likely that both BLUES and NBEs are electromagnetic manifestations of large streamer coronas (or *fast breakdown*, a term coined by Rison et al. (2016) that we also adopt here).

Some distinctive features of each type of BLUE arise from their extension and their location inside the thundercloud. For example, Soler et al. (2020) analyzed a set of 10 BLUES associated with positive NBEs and at a considerable depth inside the cloud, presumably between the main negative and the upper positive charge region of the cloud. As these events are deeply buried in the cloud, the scattering by cloud droplets and ice crystals blurs their image as observed from above, resulting in a diffuse blob that can be identified with the blue glimpses reported by Chanrion et al. (2017).

Here we focus on events that are close to the cloud top, perhaps partially outside the cloud. This location suggest an origin between the upper negative region of the cloud and the positively charged screening layer, and this is supported by radio detections that associate these events with negative-polarity NBEs (Lyu et al., 2015; Wu et al., 2012; Smith et al., 1999). Because the emissions come from close to the cloud top, optical radiation is less affected by scattering, leading to a more robust inference of source characteristics. This allows us to compare to radio observations of fast breakdown.

2 Instruments and Observations

The Modular Multispectral Imaging Array (MMIA) is a component of the Atmosphere-Space Interactions Monitor (ASIM), a mission launched on April 2, 2018 and installed on the International Space Station (Chanrion et al., 2019; Neubert et al., 2019). MMIA observes in ultraviolet and near-infrared wavelengths, points towards the nadir and contains three photometers and two cameras. The three photometers, with a temporal sampling rate of 100 kHz, include one in the UV band at 180 nm to 230 nm, and two others sensitive to the same wavelengths as two installed cameras: in the near-UV at the strongest spectral line of the nitrogen second positive system (337 nm) and at the strongest lightning emission line, OI (777.4 nm). The spatial resolution of the cameras is around $400\text{ m} \times 400\text{ m}$ at the nadir point and their integration time is 83.3 ms.

On the evening of August 7 2019, above an intense localized thunderstorm over Southern China, there were eight blue luminous events (BLUES) simultaneously detected by MMIA, the ground-based Vaisala GLD360 global lightning network and the ground-based very low frequency (VLF)/low frequency (LF) sensor at Guangzhou (see Table 1 for further details). All of them were detected by MMIA's photometer and camera filtered at 337 nm; some events had a detectable signal in the 180 nm to 230 nm photometer but there was no signal in the 777.4 nm photometer and camera at the 3σ confidence level. Depending on the event this implies that the 777.4-nm flux was at least between 50 and 300 times weaker than the 337-nm flux (see Figure A1 and the text there in Appendix A for more details). The rise times of the events in the 337 nm photometer are below $56\ \mu\text{s}$, with the shortest of them being unresolved by the $10\ \mu\text{s}$ sampling time of the photometer. The peak brightness ranges from 20 to $140\ \mu\text{W}/\text{m}^2$, which is among the brightest signals detected by MMIA. The brightness and quick rise of the events indicate that they originate close to the cloud tops or perhaps slightly above them. Note however that below we show that most of the

121 emissions were partially scattered by the cloud and that the photometer light curve is not
 122 indicative of the true source duration.

123 We sketch the context of the eight BLUEs in Figure 1 which, in panels (a) and (b), plots
 124 the intra-cloud (IC) and cloud-to-ground (CG) flashes and the eight BLUEs superimposed
 125 on the cloud top height (CTH) provided by the Fengyun-4A (FY-4A) satellite (Yang et
 126 al., 2017) for the time period from 13:04:00 to 13:07:00 UTC. During these three minutes,
 127 there were 522 lightning events with 240 CG and 282 IC flashes reported by GLD360 (see
 128 Figure 1). Two of the BLUE events (with ID 5 and 7) were missing from GLD360 so for
 129 all the BLUEs we use the location provided by the lightning location systems (LLSs) in
 130 Guangzhou province (Chen et al., 2012).

131 The absolute timing uncertainty of MMIA is on the order of tens of milliseconds but we
 132 can correct the MMIA times to sub-millisecond accuracy by comparing flash times provided
 133 by GLD360 to MMIA 777.4 nm-pulses. In our case we found that the systematic time shift
 134 with respect to the ground-based measurements experienced a time adjustment at around
 135 13:06:07, the time corrections before and after the time adjustment are (-23.3 ± 0.3) ms
 136 and (-6.2 ± 0.5) ms, respectively (see Figure B1 in Appendix B for further details). Note
 137 that the time shift -23.3 ms is similar to the estimations for other thunderstorms such as
 138 the -28.7 ms inferred by Soler et al. (2020) or the -16.37 ms from Neubert et al. (2021).

139 With this time correction we find that each of the eight BLUEs has a radio signal that,
 140 when back-propagated to the source, is within 0.7 ms of the optical peak. All VLF/LF
 141 waveforms of the BLUEs were unambiguously classified as negative NBEs measured by
 142 the vertical electric field antenna (frequency bandwidth 800 Hz to 400 kHz) located about
 143 105 km away at Guangzhou station of Jianghuai Area Sferic Array (JASA) (Qin et al., 2015;
 144 F. Liu et al., 2018).

145 Figure 1 shows in panels (c) and (d) a composition of all camera images for the BLUE
 146 events (always from the 337 nm-filtered camera). To produce this picture we have added the
 147 projection of each of the eight MMIA images into the Earth surface according to coordinates
 148 introduced by the ASIM pipeline. The resulting locations differ noticeably from those
 149 provided by LLSs and the distribution is more spread out. We attribute this to uncertainties
 150 in the camera orientation. Note also that several of the images exhibit a sharp peak that
 151 appears to emerge from the middle of the diffuse blob: this is a blooming artifact of the
 152 CCD camera.

153 To understand better the relation between the BLUE emissions and their parent thun-
 154 derstorm, we examined the progression of the cloud Top Blackbody Brightness temperature
 155 (TBB in K) provided by the Himawari-8 satellite (Bessho et al., 2016) with ten-minute
 156 resolution. Figure 2 displays the TBB around the time of our detections. The BLUE events
 157 originated from the boundary of a rapidly-evolving thunderstorm cell. This suggests that
 158 rapid turbulent mixing of the screening layer plays a role in the inception of fast breakdown
 159 (Krehbiel et al., 2008; Lyons et al., 2003) or the occurrence of groups of localized NBEs is
 160 associated with dynamically intense convection (Bandara et al., 2021). Note that the alti-
 161 tudes provided by FY-4A that we use here are likely underestimates since negative NBEs
 162 are usually associated with deep convection and detected in overshooting cloud tops (F. Liu
 163 et al., 2018; Wu et al., 2013).

164 3 Light-scattering model

165 To better understand the MMIA observations we compare them now to a simple model
 166 where the light source is a thin, straight, uniformly bright segment and the cloud is ho-
 167 mogeneous with a planar upper boundary. We neglect the intrinsic duration of the source,
 168 assuming that all light is emitted instantaneously.

Table 1. The eight BLUES simultaneously detected by MMIA, ground-based Vaisala GLD360 global lightning network and the ground-based VLF/LF sensor at Guangzhou. All the detection times have been corrected to the time with respect to the BLUES source locations.

ID	Date (Year/Month/Day)	MMIA time UTC(Source)	MMIA corrected time UTC(Source)	GLD360 time UTC(Source)	VLF/LF time UTC(Source)	Rise Time ^a (μ s)	Time duration ^b (μ s)	Peak Brightness (μ W/m ²)
1	2019/08/07	13:05:56.9362	13:05:56.9595	13:05:56.9594	13:05:56.9594	31.17	371.36	20.11
2	2019/08/07	13:05:58.6317	13:05:58.6550	13:05:58.6549	13:05:58.6549	8.04	196.72	142.18
3	2019/08/07	13:06:01.7568	13:06:01.7801	13:06:01.7800	13:06:01.7799	56.30	758.77	40.61
4	2019/08/07	13:06:09.5668	13:06:09.5730	13:06:09.5722	13:06:09.5723	8.71	399.46	97.88
5	2019/08/07	13:06:16.6329	13:06:16.6391	-	13:06:16.6384	13.07	912.33	44.51
6	2019/08/07	13:06:20.9670	13:06:20.9732	13:06:20.9726	13:06:20.9726	14.08	486.78	120.30
7	2019/08/07	13:06:30.4934	13:06:30.4996	-	13:06:30.4993	13.07	334.22	46.48
8	2019/08/07	13:06:31.6557	13:06:31.6619	13:06:31.6616	13:06:31.6615	13.40	237.87	39.96

^a Rise time is calculated using the linear interpolation by taking the time for the amplitude of a photometer signal to rise from 10% to 90%. Note that the sampling time is 10 μ s so the rise is unresolved in several events.

^b Time duration is calculated using the linear interpolation by the time interval for the amplitude of a photometer signal to rise from 10% and fall to 10%.

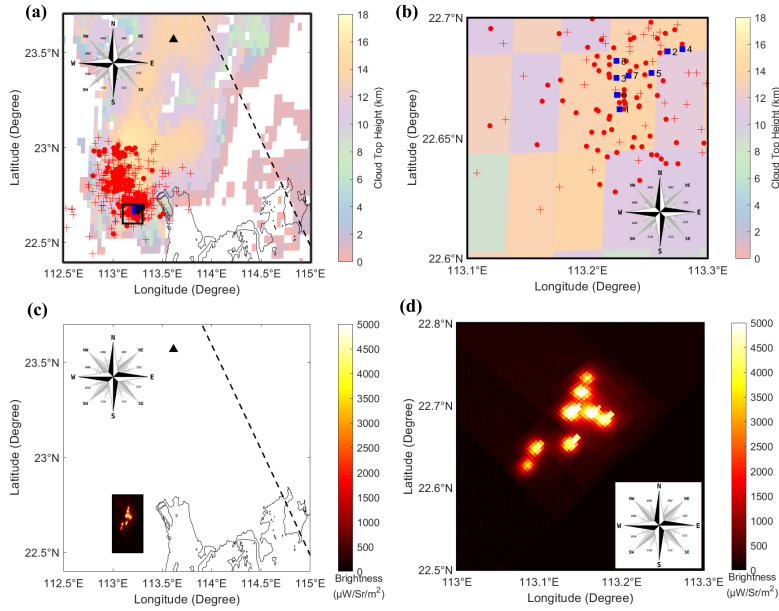


Figure 1. Distribution of the CG/IC lightning and eight BLUES along with Cloud Top Height (CTH) at the time period from 13:04:00 to 13:07:00 UTC (a) and the zoom of its black rectangular region (b) (Red dots: CG lightning detected by GLD360, Red crosses: IC lightning detected by GLD360 and Blue squares: BLUES detected by LLSs); eight BLUES images detected in the 337 nm filtered camera of MMIA (c) and the zoom (d). The ground-based VLF/LF sensor at Guangzhou is shown as black triangle. The footprints of ASIM are shown in black dashed line.

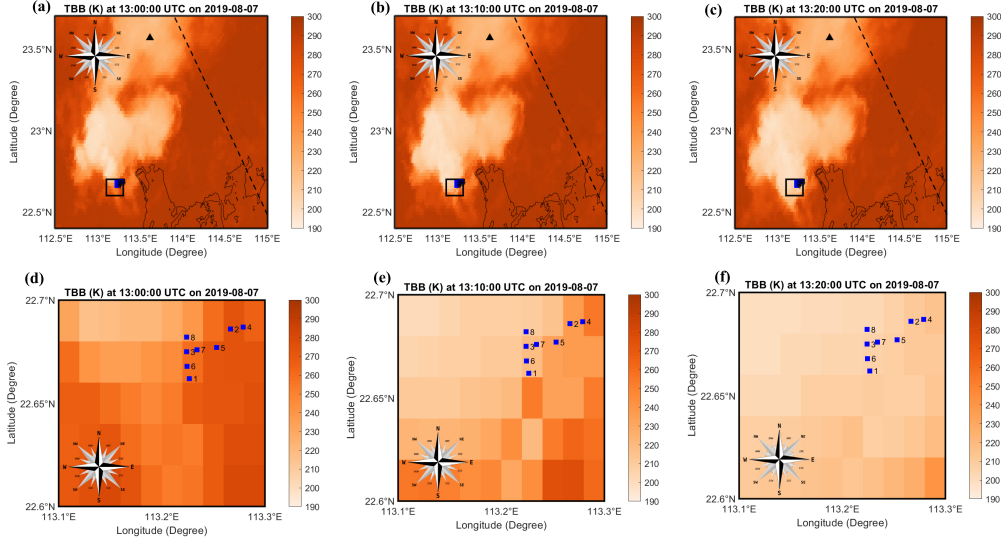


Figure 2. Cloud Top Blackbody Brightness Temperature (TBB, in K) and the zoom of its black rectangular region provided by Himawari-8 at 13:00:00 UTC (a) and (d), at 13:10:00 UTC (b) and (e), at 13:20:00 UTC (c) and (f). The ground-based VLF/LF sensor at Guangzhou is shown as black triangle. The footprints of ASIM are shown in black dashed line.

169 Because photons can be scattered many times before they exit the cloud, an impulsive
 170 optical flash results in a temporally stretched light curve. To understand this curve we
 171 start with the expression for a point-like source buried in the cloud. Using the diffusion
 172 approximation for the propagation of photons inside the cloud proposed by Koshak et al.
 173 (1994), Soler et al. (2020) gave an analytical expression for this curve, which was derived
 174 in more detail by Luque et al. (2020). Adopting the normalization and the notation of the
 175 later, the photon flux exiting the cloud top reads

$$\Gamma(t) = NF(t) = \frac{Ne^{-t/\tau_A - \tau_D/t}}{\pi^{1/2}\tau_D} \left(\frac{t}{\tau_D}\right)^{-3/2}, \quad (1)$$

176 where $F(t)$ is the flux per photon in the source, N is the total number of source photons,
 177 τ_A is the mean absorption time of the photons inside the cloud and $\tau_D = L^2/4D$ is, given
 178 a diffusion coefficient D , the characteristic time of diffusion for the distance L between
 179 the source and the cloud top. The derivation of these magnitudes from the microscopic
 180 properties of the cloud is given by Koshak et al. (1994) and reviewed by Luque et al. (2020).
 181 Equation (1) is valid for $t > 0$, where the time origin is the moment of light emission. For
 182 a distant observer, differences in light travel time from different points in the cloud are not
 183 significant so one can reinterpret the time in equation (1) with $t = 0$ being the arrival time
 184 of an unscattered photon.

185 To obtain the light curve for an extended source that spans altitudes from the cloud
 186 top to a maximum depth L_0 we integrate $(N/L_0)F(t)dL$ from 0 to L_0 (the factor N/L_0 is
 187 the linear density of source photons, assumed uniform). The result is

$$\Gamma_L(t) = N \left(\frac{D}{t}\right)^{1/2} \left(1 - e^{-\tau_D/t}\right) e^{-t/\tau_A}, \quad \tau_D = L_0^2/4D. \quad (2)$$

188 Note that this expression disregards any part of the source above the cloud top. Some
 189 photons emitted outside the cloud propagate directly to the detector and others are back-
 190 scattered by the upper cloud surface after a small number of scattering events. These

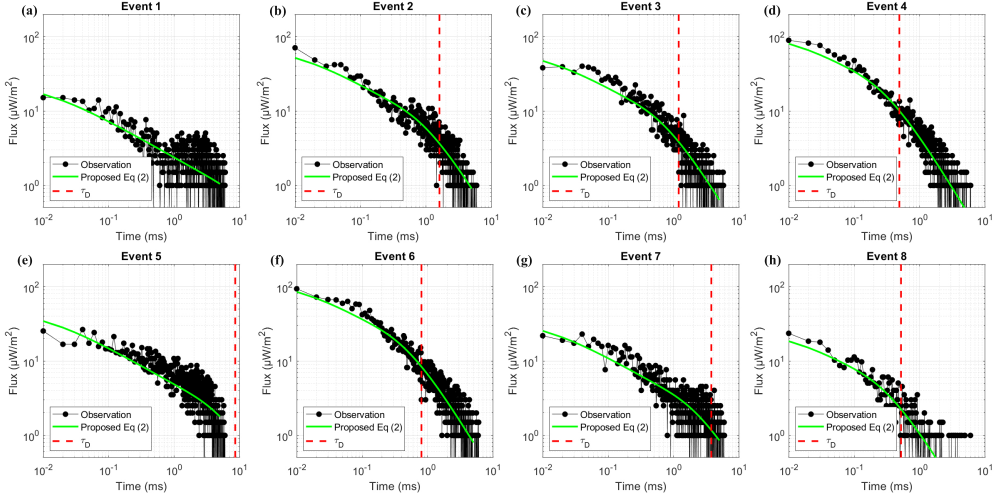


Figure 3. Comparison between MMIA observed photometer signals and those calculated by using the proposed equation (2) over the time after peak on a logarithmic scale. The best-fit cutoff time τ_D is shown in red dashed line.

191 emissions have an effect only on a few data points in a photometer with a $10\ \mu\text{s}$ time
 192 resolution. We therefore do not account for these emissions which, although may be present,
 193 do not dominate the photometer light-curves.

194 Figure 3 shows the comparison between MMIA observed photometer signals and those
 195 calculated by using the proposed equation (2) over the time after peak on a logarithmic
 196 scale. For short times after the emission, equation (2) predicts a $\sim t^{-1/2}$ dependence for the
 197 flux that is cut off by either photon absorption with a time-scale τ_A or by the finite size of the
 198 source, with a time-scale τ_D . The cutoff from the mean absorption time is likely negligible:
 199 Luque et al. (2020) estimates $\tau_A \approx 2.3\ \text{ms}$ for clouds composed by water droplets with an
 200 effective radius of $20\ \mu\text{m}$ and a droplet density of $10^8\ \text{m}^{-3}$ but this possibly overestimates
 201 the absorption. The cloud tops are dominated by ice particles, which absorb radiation at
 202 $337\ \text{nm}$ several orders of magnitude less efficiently than water (Warren & Brandt, 2008).
 203 Besides, the available estimates of the extinction coefficient (Peterson, 2020; Platt, 1997)
 204 also lead to absorption times significantly longer than the duration of our events. Hence
 205 here we assume $\tau_A \gg \tau_D$.

206 As we show in Figure 3, most of the recorded BLUEs light-curves have the shape
 207 predicted by equation (2). In the figure we plot a least-squares fit of the observational data
 208 to the model with two parameters: an overall amplitude factor and the decay time τ_D . To
 209 reduce the effect of the emissions from outside the cloud discussed above, we disregard the
 210 data points at the peak of the light-curve. The good fit of most events indicate that indeed
 211 they originate from sources that extend below the cloud top. Event 5 is the only one that
 212 does not show a clear $t^{-1/2}$ decay, possibly because there was a gap between the source and
 213 the cloud top or because light emissions were inhomogeneous or long-lasting. In events 1
 214 and 7 there is weak secondary activity 1 ms to 2 ms after the main peak that distorts the
 215 estimate of the cutoff time τ_D .

216 From Table 2, leaving aside events where τ_D was estimated poorly, this cutoff time
 217 ranges between 0.5 ms and 1.6 ms. The smallest diffusion coefficient proposed by Soler et al.
 218 (2020), $D = 3 \times 10^9\ \text{m}^2\text{s}^{-1}$ yields a range of lengths for the optical sources of $L_0 = 2.4\ \text{km}$
 219 to 4.4 km. However, the evaluated results will be affected by the uncertainties that surround
 220 our modeling of the cloud composition.

Table 2. Model-inferred properties of the eight BLUE events. We list the cloud top height measured by FY-4A at the event location, the best-fit cutoff time τ_D (see equation (2)), the resulting source length $L_0 = (4D\tau_D)^{1/2}$ with $D = 3 \times 10^9 \text{ m}^2\text{s}^{-1}$, the total optical energy in the 337-nm band of the second positive system of nitrogen and an estimation of the number of streamer branching events in the fast breakdown processes that we assume that originated the events.

ID	Cloud top height (km)	Cutoff time (τ_D) (ms)	Source length (L_0) (km)	Optical energy at 337 nm (J)	Branching events
1	11.2	19.6 ^a	- ^a	1.8×10^4	1.4×10^9
2	11.6	1.6	4.4	1.9×10^4	1.4×10^9
3	14.0	1.2	3.8	1.2×10^4	9.1×10^8
4	13.1	0.5	2.4	1.3×10^4	9.8×10^8
5	11.6	8.6 ^b	- ^b	2.4×10^4	1.9×10^9
6	14.0	0.8	3.1	1.8×10^4	1.4×10^9
7	14.0	3.8 ^a	- ^a	1.6×10^4	1.2×10^9
8	14.0	0.5	2.5	4.6×10^3	3.6×10^8

^a In events 1 and 7 there is secondary activity that distorted the estimation of the cutoff time τ_D and the source length.

^b Event 5 has a light-curve that cannot be explained by an impulsive, uniformly bright source.

221 Next we extend our model to include the propagation of the signal to the MMIA
 222 instruments, accounting for Rayleigh scattering by the atmosphere and for the non-isotropic
 223 (approximately Lambertian) emission pattern from the cloud tops. We use the radiative
 224 transfer Monte Carlo code CloudScat.jl (Luque et al., 2020) and run simulations of uniformly
 225 bright, straight vertical sources, with the lengths L_0 derived above, in a homogeneous cloud
 226 that spans altitudes from 7 km to the cloud top height derived by the Fengyun-4A (FY-4A)
 227 satellite (listed in Table 2). The scattering parameters in the cloud are those for a density of
 228 10^8 m^{-3} spherical ice particles with 20 μm radius. The relative positions between the source
 229 and the observer reproduce the conditions of each of the eight BLUEs in our dataset.

230 In Figure 4 we show the results of the Monte Carlo code comparing with 337-nm
 231 photometer and camera observations for the event 2 and 8 (Additional comparisons can be
 232 found in Figure S1-S8 in Supplemental material). The photometer light curves calculated
 233 from CloudScat model closely follow the analytical estimate of equation (2) and are a good
 234 fit to the observations. The simulated camera images are also reasonably close to MMIA's
 235 records although they are slightly more compact. This is a possible indication of a non-
 236 negligible source width on the order of the camera resolution of about 400 m.

237 In the results presented here we always consider that the top of the source coincides
 238 with the top of the cloud. As we discuss above, the effect of light emissions outside the cloud
 239 is too impulsive to compare against the MMIA photometer and is possibly dominated by the
 240 intrinsic time-dependence of the source. We performed additional Monte Carlo simulations
 241 that confirm that the photometer light-curves are compatible with source tops within a
 242 few hundred meters of the cloud top, either above or below it. The VLF/LF waveforms of
 243 negative NBEs for event 2 and 8 are also shown in Figure 4. The radio signals of the eight
 244 events, along with other positive NBEs at deeper locations in the same thunderstorm, are
 245 analyzed with more details in a complementary publication (F. Liu et al., 2021).

246 The CloudScat.jl code outputs a photon flux at the observer's location in units of photons
 247 per unit time and unit surface that reach a detector for each photon in the source
 248 whereas the MMIA photometers are calibrated in terms of power per unit surface (irradiance).
 249 The conversion factor is the total energy of the event in the 337 band, $E = Nhc/\lambda$,
 250 where N is the total number of photons emitted by the source, h is the Planck's constant, c
 251 is the speed of light and $\lambda = 337 \text{ nm}$. By comparing the results of our Monte Carlo code to
 252 the MMIA data we found the best-matching total energy of each event. Because the events

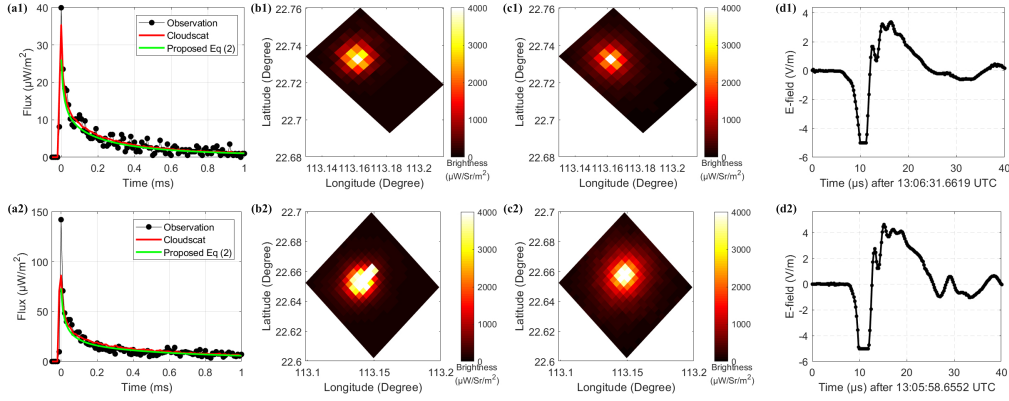


Figure 4. Comparing the modeling results against the observation of MMIA for event 8 (a1 - d1) and event 2 (a2 - d2). The 337 nm photometer signals (a1, a2): MMIA observation (black dotted line), modeling results by using CloudScat model (red line) and the proposed equation (2) (green line). The images measured by 337 nm filtered camera of MMIA (b1, b2). The simulated images obtained from CloudScat model (c1, c2). The waveforms of the NBEs detected from the ground-based VLF/LF sensor at Guangzhou (d1, d2).

253 that we analyze are close to the cloud tops and thus barely affected by in-cloud absorption,
 254 our estimates of E are weakly sensitive to our model assumptions and thus provide a rea-
 255 sonably precise picture of the actual source emission intensity of the BLUE events. The
 256 estimated energies are listed in Table 2.

257 N. Liu et al. (2019) analyzed radio spectra of NBEs and concluded that they can be
 258 understood as systems of 10^7 to 10^8 streamers. In that analysis the key feature of a streamer
 259 is a current moment that increases rapidly on a time scale of about one nanosecond, which
 260 is the timescale of streamer initiation in numerical simulations. Here we also consider
 261 that a single nanosecond event may produce more than one streamer, as is the case in a
 262 bifurcated tree. Denoting by b the mean number of streamers emerging from an event, we
 263 have $M = bK$, where M is the total number of streamers (unbifurcated branches) and K is
 264 the number of initiation events (most likely bifurcations from other streamers). Then the
 265 total streamer length contained in one fast breakdown process is ℓbK , where ℓ is the mean
 266 length between bifurcations (but see Nijdam et al. (2020) for a discussion of the difficulties
 267 involved in precisely defining this quantity). If a streamer emits η photons per unit length
 268 as it propagates, the total number of emitted photons is $N = \eta \ell bK$.

269 It follows from the scaling laws for streamers (Ebert et al., 2010) that η depends on
 270 air density only through collisional quenching of the radiative states of N_2 (the remaining
 271 factor is proportional to $\pi R^2 n_e$ where R is the streamer radius, which scales as the inverse
 272 of air density, and n_e is the electron density, which scales as the square of air density). The
 273 numerical simulations by Malagón-Romero & Luque (2019) predict a time-integrated photon
 274 yield of about $2 \times 10^{18} \text{ m}^{-3}$ in a streamer of radius $R \approx 2 \text{ mm}$. From the spectra presented
 275 by F. J. Gordillo-Vázquez et al. (2012), we infer that about 30% of these emissions are inside
 276 the 5-nm window of the 337-nm MMIA photometer, yielding $\eta \approx (n_0/n) \times 2 \times 10^{12} \text{ m}^{-1}$,
 277 where n_0/n is the ratio of air density at atmospheric-pressure, n_0 , to the density at the
 278 altitude of interest, n . Here we take $n_0/n \approx 6$ for an altitude of 14 km. Briels et al. (2008)
 279 observed a ratio of branching length to streamer radius of about 20, so a radius of 2 mm
 280 at atmospheric pressure translates into $\ell \approx (n_0/n) \times 4 \text{ cm} = 24 \text{ cm}$. We take the branching
 281 number b to be 2, although there are evidences that it may possibly be larger (Heijmans et
 282 al., 2013, 2015).

283 The estimation of the number of streamer branches for all the BLUEs are listed in
 284 Table 2. Our results are 10-100 times above those derived from radio spectra by N. Liu et
 285 al. (2019). One possible reason for this disagreement is the uncertainties in our assumed
 286 parameters. For example, the estimated K is highly sensitive to the assumed streamer
 287 radius: had we chosen a radius of 5 mm at atmospheric pressure, the estimation of K would
 288 be reduced by about a factor 15. It is also possible that a large fraction of the optical signal
 289 in fast breakdown is emitted not close to streamer heads but from long-lived glows, as is
 290 the case in sprites (Luque et al., 2016; Pérez-Invernón et al., 2020).

291 4 Discussion and conclusions

292 The eight BLUE events that we analyze in this paper expand and complete the picture
 293 of fast breakdown as the source of both optical blue-dominated emissions and radio pulses
 294 detected as NBEs in the VLF/LF bands or high-amplitude noise in VHF. All events were
 295 strongly detected in the photometer and camera filtered at 337 nm; in some events there was
 296 a weak signal in 180-230 nm but with no signal in 777.4 nm photometer and camera.

297 As in previous studies (Wescott et al., 1995, 1996; Chanrion et al., 2017), the BLUEs
 298 appeared temporally isolated from either CG or IC flashes detected by the GLD360 network.
 299 However, all the BLUEs coincide with NBEs observed by the ground-based VLF/LF sensor
 300 at Guangzhou. This strengthens the connection between BLUEs and negative NBEs (Chou
 301 et al., 2018; F. Liu et al., 2018) and further supports that NBEs originate from non-thermal,
 302 streamer processes (Rison et al., 2016; Lyu et al., 2019; Tilles et al., 2019; Soler et al., 2020).

303 The rise times of the blue events in the 337 nm photometer are between 10 μ s to 70 μ s
 304 with peak irradiance varying from 20 μ Wm⁻² to 140 μ Wm⁻². The brightness and short rise
 305 times suggest a source close or even slightly above the cloud tops and this is supported by
 306 our modeling results based either on the diffusion approximation by Koshak et al. (1994) or
 307 on a Monte Carlo radiative transfer code (Luque et al., 2020). Since all events are identified
 308 as negative NBEs, this is consistent with previous studies that localize the initiation of most
 309 of negative NBEs between the upper positive charge region and the screening charge region
 310 of the thunderstorm (Smith et al., 1999; Wu et al., 2012; Lyu et al., 2015). The variation
 311 in the rise times between different events may be due to differences in the intrinsic time
 312 dependence of the optical sources but this is equally well explained by a finite distance to
 313 the cloud top or from non-uniformities of the optical sources below the cloud.

314 Our estimates of the total optical energy within the 337-nm band provide a new con-
 315 straint for models of fast breakdown. The present understanding of these events is still
 316 limited and it is difficult to translate this energy into microscopical properties of fast break-
 317 down. However our results confirm that fast breakdown involves more than 10^7 streamers,
 318 as inferred by N. Liu et al. (2019) and further analyzed by Cooray et al. (2020).

319 Future investigations should address the underlying physics of fast breakdown and its
 320 global significance, including its relation to lightning initiation. Data from the ASIM mission
 321 will likely play a decisive role in this research.

322 Appendix

323 Appendix A Constraints in the 777.4-nm emission for Blue Luminous 324 Events (BLUEs)

325 To establish rigorous bounds to the possible signal in the 777.4-nm photometer we pro-
 326 ceeded as follows. For each event first we divided the photometer light-curve into temporal
 327 bins of $m = 40$ samples (0.4 ms) and computed the mean inside each bin b as

$$Y_b = \frac{1}{m} \sum_{i=k_b \dots k_b+m-1} y_i, \quad (\text{A1})$$

328 where k_b is the earliest sample inside b and y_i is the value of each sample. These $Y_b = S_b + \eta_b$
 329 contain a possible signal from the observed events S_b as well as stochastic background noise
 330 η_b . To characterize the statistical distribution of η_b we find a bin where we can assume
 331 $S_b = 0$ by selecting the bin with the largest Y_b below the median of all Y_b . We computed
 332 the empirical average μ_1 and standard deviation σ_1 for the samples inside this background
 333 bin. Then we approximate the distribution function of η_b as a Gaussian with mean $\mu = \mu_1$
 334 and standard deviation $\sigma = \sigma_1/\sqrt{m}$. Hence we can mark bins with signals Y_b above $\mu + 3\sigma$
 335 as statistically significant (p -value < 0.0014).

336 The fact that we did not have any statistically significant 777.4-nm observation coincid-
 337 ing with the 337-nm peaks implies that in all cases the 777.4-nm signal was, if it existed,
 338 weaker than $0.4 \mu\text{W}/\text{m}^2$, which was between 50 and 300 times below the 337-nm peaks for
 339 different cases.

340 On the other hand there were statistically significant emissions detected by the UV
 341 photometer sensitive to wavelengths in 180-230 nm. From our 8 events, 3 had UV detections
 342 coinciding with the 337-nm peaks at the 3σ level (events with ID 2, 3 and 5), 2 of them at
 343 the 5σ level (events with ID 4 and 6).

344 In Figure A1 we show the signals of the three photometers corresponding to event 6 in
 345 Tables 1 and 2 of the main text. This is the event with the strongest UV signal.

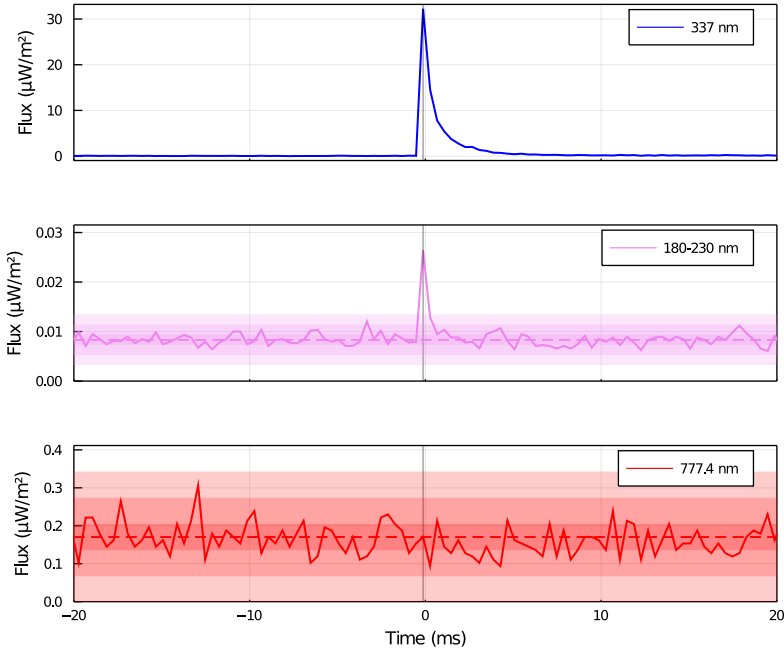


Figure A1. Signals from the three MMIA photometers for event 6, binned in intervals of 40 samples (0.4 ms). For 180-230 nm and 777.4 nm we also show an approximation to the background noise as described in the text: the horizontal, dashed line is the expected value μ and the shaded bands indicate $\mu \pm \sigma$, $\mu \pm 3\sigma$ and $\mu \pm 5\sigma$.

346 **Appendix B The systematic time shift of MMIA with respect to the**
 347 **ground-based measurements**

348 The systematic time shift of MMIA is estimated by using the 777-nm pulses and their
 349 simultaneous GLD360 events, which are (-23.3 ± 0.3) ms and (-6.2 ± 0.5) ms before and
 350 after the time adjustment τ , see Figure B1 for details.

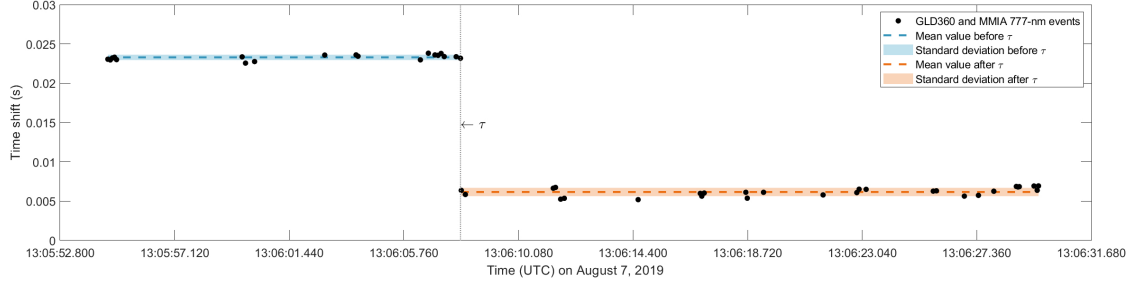


Figure B1. The systematic time shift of MMIA with respect to the ground-based measurements calculated by using MMIA 777-nm pulses and their simultaneous GLD360 events. The time shift experienced a time adjustment at τ around 13:06:07 (see black dashed line). The mean value before and after τ are -23.3 ms and -6.2 ms with the standard deviation ± 0.3 ms and ± 0.5 ms, respectively.

Acknowledgments

This work was supported by the European Research Council (ERC) under the European Union H2020 programme/ERC grant agreement 681257. It also received funding from the European Union Horizon 2020 research and innovation programme under the Marie Skłodowska-Curie grant agreement SAINT 722337. Additionally, this work was supported by the Spanish Ministry of Science and Innovation, MINECO, under project PID2019-109269RB-C43 and FEDER program. DL, AL and FJGV acknowledge financial support from the State Agency for Research of the Spanish MCIU through the 'Center of Excellence Severo Ochoa' award for the Instituto de Astrofísica de Andalucía (SEV-2017-0709). FL, GL and BZ are supported by the National Key Research and Development Program of China (2017YFC1501501) and National Natural Science Foundation of China (41775004, 41875006, 42005068, U1938115). The Modular Multispectral Imaging Array (MMIA) data and Global Lightning Detection Network GLD360 data used in this study were obtained at (<https://asdc.space.dtu.dk/>). The cloud top height data is based on the data sharing proxy in Fengyun Satellite data center (<http://satellite.nsmc.org.cn/PortalSite/Data/Satellite.aspx?currentculture=en-US>). The Himawari-8 gridded data in this study is supplied by the P-Tree System, Japan Aerospace Exploration Agency (JAXA)/Earth Observation Research Center (EORC) (<https://www.eorc.jaxa.jp/ptree/>). The data that support the findings of this study are openly available in (<http://doi.org/10.5281/zenodo.4588549>).

References

- Bandara, S., Marshall, T., Karunarathne, S., & Stolzenburg, M. (2021). Groups of narrow bipolar events within thunderstorms. *Atmospheric Research*, *252*, 105450. doi: <https://doi.org/10.1016/j.atmosres.2021.105450>
- Bessho, K., Date, K., Hayashi, M., Ikeda, A., Imai, T., Inoue, H., ... others (2016). An introduction to Himawari-8/9—Japan's new-generation geostationary meteorological satellites. *Journal of the Meteorological Society of Japan. Ser. II*, *94*(2), 151–183.
- Boeck, W. L., Vaughan, O. H., Blakeslee, R., Vonnegut, B., & Brook, M. (1998). The role of the space shuttle videotapes in the discovery of sprites, jets and elves. *Journal of Atmospheric and Solar-Terrestrial Physics*, *60*(7), 669 - 677. doi: [https://doi.org/10.1016/S1364-6826\(98\)00025-X](https://doi.org/10.1016/S1364-6826(98)00025-X)
- Briels, T. M. P., van Veldhuizen, E. M., & Ebert, U. (2008, nov). Positive streamers in air and nitrogen of varying density: experiments on similarity laws. *Journal of Physics D: Applied Physics*, *41*(23), 234008. doi: 10.1088/0022-3727/41/23/234008
- Chanrion, O., Neubert, T., Mogensen, A., Yair, Y., Stendel, M., Singh, R., & Siingh, D. (2017). Profuse activity of blue electrical discharges at the tops of thunderstorms. *Geophysical Research Letters*, *44*(1), 496-503. doi: <https://doi.org/10.1002/2016GL071311>
- Chanrion, O., Neubert, T., Rasmussen, I. L., Stoltze, C., Tcherniak, D., Jessen, N. C., ... others (2019). The modular multispectral imaging array (MMIA) of the ASIM payload on the international space station. *Space Science Reviews*, *215*(4), 1–25.
- Chen, L., Zhang, Y., Lu, W., Zheng, D., Zhang, Y., Chen, S., & Huang, Z. (2012). Performance evaluation for a lightning location system based on observations of artificially triggered lightning and natural lightning flashes. *Journal of Atmospheric and Oceanic Technology*, *29*(12), 1835–1844.
- Chou, J. K., Hsu, R.-R., Su, H.-T., Chen, A. B.-C., Kuo, C.-L., Huang, S.-M., ... Wu, Y.-J. (2018). ISUAL-observed blue luminous events: The associated sferics. *Journal of Geophysical Research: Space Physics*, *123*(4), 3063-3077. doi: <https://doi.org/10.1002/2017JA024793>
- Chou, J. K., Tsai, L. Y., Kuo, C. L., Lee, Y. J., Chen, C. M., Chen, A. B., ... Lee, L. C. (2011). Optical emissions and behaviors of the blue starters, blue jets, and gigantic jets observed in the taiwan transient luminous event ground campaign. *Journal of Geophysical Research: Space Physics*, *116*(A7).

- 403 Cooray, V., Cooray, G., Rubinstein, M., & Rachidi, F. (2020). Modeling compact intracloud
404 discharge (CID) as a streamer burst. *Atmosphere*, *11*(5). doi: 10.3390/atmos11050549
- 405 Ebert, U., Nijdam, S., Li, C., Luque, A., Briels, T., & van Veldhuizen, E. (2010). Review
406 of recent results on streamer discharges and discussion of their relevance for sprites and
407 lightning. *Journal of Geophysical Research: Space Physics*, *115*(A7). doi: [https://doi.org/](https://doi.org/10.1029/2009JA014867)
408 [10.1029/2009JA014867](https://doi.org/10.1029/2009JA014867)
- 409 Edens, H. E. (2011). Photographic and lightning mapping observations of a blue starter
410 over a new mexico thunderstorm. *Geophysical Research Letters*, *38*(17). doi: [https://](https://doi.org/10.1029/2011GL048543)
411 doi.org/10.1029/2011GL048543
- 412 Gordillo-Vázquez, F., & Pérez-Invernón, F. (2021). A review of the impact of transient
413 luminous events on the atmospheric chemistry: Past, present, and future. *Atmospheric*
414 *Research*, *252*, 105432. doi: <https://doi.org/10.1016/j.atmosres.2020.105432>
- 415 Gordillo-Vázquez, F. J., Luque, A., & Simek, M. (2012). Near infrared and ultraviolet
416 spectra of TLEs. *Journal of Geophysical Research: Space Physics*, *117*(A5). doi: [https://](https://doi.org/10.1029/2012JA017516)
417 doi.org/10.1029/2012JA017516
- 418 Heijmans, L. C. J., Clevis, T., Nijdam, S., Van Veldhuizen, E., & Ebert, U. (2015). Streamer
419 knotwilg branching: sudden transition in morphology of positive streamers in high-purity
420 nitrogen. *Journal of Physics D: Applied Physics*, *48*(35), 355202.
- 421 Heijmans, L. C. J., Nijdam, S., van Veldhuizen, E. M., & Ebert, U. (2013, jul). Streamers
422 in air splitting into three branches. *EPL (Europhysics Letters)*, *103*(2), 25002. doi:
423 [10.1209/0295-5075/103/25002](https://doi.org/10.1209/0295-5075/103/25002)
- 424 Koshak, W. J., Solakiewicz, R. J., Phanord, D. D., & Blakeslee, R. J. (1994). Diffusion
425 model for lightning radiative transfer. *Journal of Geophysical Research: Atmospheres*,
426 *99*(D7), 14361-14371. doi: <https://doi.org/10.1029/94JD00022>
- 427 Krehbiel, P. R., Rioussel, J. A., Pasko, V. P., Thomas, R. J., Rison, W., Stanley, M. A.,
428 & Edens, H. E. (2008). Upward electrical discharges from thunderstorms. *Nature Geo-*
429 *science*, *1*(4), 233–237.
- 430 Kuo, C.-L., Hsu, R. R., Chen, A. B., Su, H. T., Lee, L. C., Mende, S. B., ... Takahashi,
431 Y. (2005). Electric fields and electron energies inferred from the ISUAL recorded sprites.
432 *Geophysical Research Letters*, *32*(19). doi: <https://doi.org/10.1029/2005GL023389>
- 433 Liu, F., Lu, G., Neubert, T., Lei, J., Chanrion, O., Østgaard, N., ... Zhu, B. (2021). Optical
434 emissions associated with narrow bipolar events in radio signals from thunderstorms.
435 *Submitted to Nature communications*. Retrieved from [https://www.researchsquare](https://www.researchsquare.com/article/rs-311122/v1)
436 [.com/article/rs-311122/v1](https://www.researchsquare.com/article/rs-311122/v1) doi: 10.21203/rs.3.rs-311122/v1
- 437 Liu, F., Zhu, B., Lu, G., Qin, Z., Lei, J., Peng, K.-M., ... others (2018). Observations of
438 blue discharges associated with negative narrow bipolar events in active deep convection.
439 *Geophysical Research Letters*, *45*(6), 2842–2851.
- 440 Liu, N., Dwyer, J. R., Tilles, J. N., Stanley, M. A., Krehbiel, P. R., Rison, W., ... Wilson,
441 J. G. (2019). Understanding the radio spectrum of thunderstorm narrow bipolar events.
442 *Journal of Geophysical Research: Atmospheres*, *124*(17-18), 10134-10153. doi: [https://](https://doi.org/10.1029/2019JD030439)
443 doi.org/10.1029/2019JD030439
- 444 Luque, A., Gordillo-Vázquez, F. J., Li, D., Malagón-Romero, A., Pérez-Invernón, F. J.,
445 Schmalzried, A., ... Østgaard, N. (2020). Modeling lightning observations from space-
446 based platforms (Cloudscat.jl 1.0). *Geoscientific Model Development*, *13*(11), 5549–5566.
447 doi: 10.5194/gmd-13-5549-2020
- 448 Luque, A., Stenbaek-Nielsen, H. C., McHarg, M. G., & Haaland, R. K. (2016). Sprite
449 beads and glows arising from the attachment instability in streamer channels. *Journal of*
450 *Geophysical Research: Space Physics*, *121*(3), 2431-2449. doi: [https://doi.org/10.1002/](https://doi.org/10.1002/2015JA022234)
451 [2015JA022234](https://doi.org/10.1002/2015JA022234)
- 452 Lyons, W. A., Nelson, T. E., Armstrong, R. A., Pasko, V. P., & Stanley, M. A. (2003).
453 Upward electrical discharges from thunderstorm tops. *Bulletin of the American Meteorolo-*
454 *gical Society*, *84*(4), 445–454.
- 455 Lyu, F., Cummer, S. A., & McTague, L. (2015). Insights into high peak current in-cloud
456 lightning events during thunderstorms. *Geophysical Research Letters*, *42*(16), 6836-6843.

- doi: <https://doi.org/10.1002/2015GL065047>
- 457
458 Lyu, F., Cummer, S. A., Qin, Z., & Chen, M. (2019). Lightning initiation processes imaged
459 with very high frequency broadband interferometry. *Journal of Geophysical Research:*
460 *Atmospheres*, *124*(6), 2994–3004. doi: <https://doi.org/10.1029/2018JD029817>
- 461 Malagón-Romero, A., & Luque, A. (2019). Spontaneous emergence of space stems ahead
462 of negative leaders in lightning and long sparks. *Geophysical Research Letters*, *46*(7),
463 4029–4038. doi: <https://doi.org/10.1029/2019GL082063>
- 464 Neubert, T., Chanrion, O., Heumesser, M., Dimitriadou, K., Husbjerg, L., Rasmussen,
465 I. L., . . . Reglero, V. (2021). Observation of the onset of a blue jet into the stratosphere.
466 *Nature*, *589*(7842), 371–375.
- 467 Neubert, T., Østgaard, N., Reglero, V., Blanc, E., Chanrion, O., Oxborrow, C. A., . . .
468 Bhandari, D. D. (2019). The ASIM mission on the international space station. *Space*
469 *Science Reviews*, *215*(2), 1–17.
- 470 Nijdam, S., Teunissen, J., & Ebert, U. (2020, Nov). The physics of streamer discharge
471 phenomena. *Plasma Sources Science and Technology*, *29*(10), 103001. doi: 10.1088/
472 1361-6595/abaa05
- 473 Pasko, V. P. (2008, nov). Blue jets and gigantic jets: transient luminous events between
474 thunderstorm tops and the lower ionosphere. *Plasma Physics and Controlled Fusion*,
475 *50*(12), 124050. doi: 10.1088/0741-3335/50/12/124050
- 476 Peterson, M. (2020). Modeling the transmission of optical lightning signals through
477 complex 3-D cloud scenes. *Journal of Geophysical Research: Atmospheres*, *125*(23),
478 e2020JD033231. (e2020JD033231 2020JD033231) doi: [https://doi.org/10.1029/](https://doi.org/10.1029/2020JD033231)
479 [2020JD033231](https://doi.org/10.1029/2020JD033231)
- 480 Platt, C. M. R. (1997). A parameterization of the visible extinction coefficient of ice clouds
481 in terms of the ice/water content. *Journal of Atmospheric Sciences*, *54*(16), 2083–2098.
- 482 Pérez-Invernón, F. J., Malagón-Romero, A., Gordillo-Vázquez, F. J., & Luque, A. (2020).
483 The contribution of sprite streamers to the chemical composition of the mesosphere-lower
484 thermosphere. *Geophysical Research Letters*, *47*(14), e2020GL088578. (e2020GL088578
485 10.1029/2020GL088578) doi: <https://doi.org/10.1029/2020GL088578>
- 486 Qin, Z., ZHU, B., MA, M., MA, D., et al. (2015). Using time domain waveforms of
487 return strokes to retrieve the daytime fluctuation of ionospheric D layer. *Chinese Science*
488 *Bulletin*, *60*(7), 654–663.
- 489 Rison, W., Krehbiel, P. R., Stock, M. G., Edens, H. E., Shao, X.-M., Thomas, R. J., . . .
490 Zhang, Y. (2016). Observations of narrow bipolar events reveal how lightning is initiated
491 in thunderstorms. *Nature communications*, *7*(1), 1–12.
- 492 Smith, D. A., Shao, X. M., Holden, D. N., Rhodes, C. T., Brook, M., Krehbiel, P. R.,
493 . . . Thomas, R. J. (1999). A distinct class of isolated intracloud lightning discharges
494 and their associated radio emissions. *Journal of Geophysical Research: Atmospheres*,
495 *104*(D4), 4189–4212. doi: <https://doi.org/10.1029/1998JD200045>
- 496 Soler, S., Pérez-Invernón, F. J., Gordillo-Vázquez, F. J., Luque, A., Li, D., Malagón-Romero,
497 A., . . . Østgaard, N. (2020). Blue optical observations of narrow bipolar events by ASIM
498 suggest corona streamer activity in thunderstorms. *Journal of Geophysical Research:*
499 *Atmospheres*, *125*(16), e2020JD032708. (e2020JD032708 10.1029/2020JD032708) doi:
500 <https://doi.org/10.1029/2020JD032708>
- 501 Surkov, V. V., & Hayakawa, M. (2020). Progress in the study of transient luminous and
502 atmospheric events: A review. *Surveys in Geophysics*, *41*, 1101–1142.
- 503 Tilles, J. N., Liu, N., Stanley, M. A., Krehbiel, P. R., Rison, W., Stock, M. G., . . . Wilson,
504 J. (2019). Fast negative breakdown in thunderstorms. *Nature communications*, *10*(1),
505 1–12.
- 506 van der Velde, O. A., Montanyà, J., López, J. A., & Cummer, S. A. (2019). Gigantic
507 jet discharges evolve stepwise through the middle atmosphere. *Nature communications*,
508 *10*(1), 1–10.
- 509 Warren, S. G., & Brandt, R. E. (2008). Optical constants of ice from the ultraviolet to
510 the microwave: A revised compilation. *Journal of Geophysical Research: Atmospheres*,

- 511 113(D14). doi: <https://doi.org/10.1029/2007JD009744>
- 512 Wescott, E. M., Sentman, D., Osborne, D., Hampton, D., & Heavner, M. (1995). Preliminary
513 results from the Sprites94 aircraft campaign: 2. blue jets. *Geophysical Research Letters*,
514 22(10), 1209-1212. doi: <https://doi.org/10.1029/95GL00582>
- 515 Wescott, E. M., Sentman, D. D., Heavner, M. J., Hampton, D. L., Osborne, D. L., &
516 Vaughan Jr., O. H. (1996). Blue starters brief upward discharges from an intense arkansas
517 thunderstorm. *Geophysical Research Letters*, 23(16), 2153-2156. doi: <https://doi.org/10.1029/96GL01969>
- 518
- 519 Wescott, E. M., Sentman, D. D., Stenbaek-Nielsen, H. C., Huet, P., Heavner, M. J., &
520 Moudry, D. R. (2001). New evidence for the brightness and ionization of blue starters
521 and blue jets. *Journal of Geophysical Research: Space Physics*, 106(A10), 21549-21554.
522 doi: <https://doi.org/10.1029/2000JA000429>
- 523 Wu, T., Dong, W., Zhang, Y., Funaki, T., Yoshida, S., Morimoto, T., ... Kawasaki, Z.
524 (2012). Discharge height of lightning narrow bipolar events. *Journal of Geophysical*
525 *Research: Atmospheres*, 117(D5). doi: <https://doi.org/10.1029/2011JD017054>
- 526 Wu, T., Takayanagi, Y., Yoshida, S., Funaki, T., Ushio, T., & Kawasaki, Z. (2013). Spatial
527 relationship between lightning narrow bipolar events and parent thunderstorms as revealed
528 by phased array radar. *Geophysical Research Letters*, 40(3), 618-623. doi: <https://doi.org/10.1002/grl.50112>
- 529
- 530 Yang, J., Zhang, Z., Wei, C., Lu, F., & Guo, Q. (2017). Introducing the new generation of
531 chinese geostationary weather satellites, fengyun-4. *Bulletin of the American Meteorolog-*
532 *ical Society*, 98(8), 1637-1658.